Inorganic Chemistry

ARTICLE

pubs.acs.org/IC

Theoretical Study of Oxidation of Cyclohexane Diol to Adipic Anhydride by $[Ru^{IV}(O)(tpa)(H_2O)]^{2+}$ Complex (tpa = Tris(2-pyridylmethyl)amine)

Yoshihito Shiota,[†] Jorge M. Herrera,[†] Gergely Juhász,[†] Takafumi Abe,[†] Shingo Ohzu,[‡] Tomoya Ishizuka,[‡] Takahiko Kojima,[‡] and Kazunari Yoshizawa*[,†]

[†]Institute for Materials Chemistry and Engineering and International Research Center for Molecular System, Kyushu University, Fukuoka 819-0395, Japan

[‡]Department of Chemistry, Graduate School of Pure and Applied Sciences, University of Tsukuba, Ibaraki 305-8571, Japan

Supporting Information

ABSTRACT: The catalytic conversion of 1,2-cyclohexanediol to adipic anhydride by $Ru^{IV}O(tpa)$ (tpa = tris(2-pyridylmethyl)amine) is discussed using density functional theory calculations. The whole reaction is divided into three steps: (1) formation of α-hydroxy cyclohexanone by dehydrogenation of cyclohexanediol, (2) formation of 1,2-cyclohexanedione by dehydrogenation of α-hydroxy cyclohexanone, and (3) formation of adipic anhydride by oxygenation of cyclohexanedione. In each step the two-electron oxidation is performed by $Ru^{IV}O(tpa)$ active species, which is reduced to bis-aqua $Ru^{II}(tpa)$ complex. The Ru^{II} complex is reactivated using Ce(IV) and water as an oxygen source. There are two different pathways of the first two steps of the conversion depending on whether the direct H-atom abstraction occurs on a C−H bond or on its adjacent oxygen O−H. In the first step, the C−H (O−H) bond dissociation occurs in **TS1** (**TS2**−**1**) with an activation barrier of 21.4 (21.6) kcal/mol, which is followed by abstraction of another hydrogen with the spin transition in both pathways. The second process also bifurcates into two reaction pathways. **TS3** (**TS4**−**1**) is leading to dissociation of the C−H (O−H) bond, and the activation barrier of **TS3** (**TS4**−**1**) is 20.2 (20.7) kcal/mol. In the third step, oxo ligand attack on the carbonyl carbon and hydrogen migration from the water ligand occur via **TS5** with an activation barrier of 17.4 kcal/mol leading to a stable tetrahedral intermediate in a triplet state. However, the slightly higher energy singlet state of this tetrahedral intermediate is unstable; therefore, a spin crossover spontaneously transforms the tetrahedral intermediate into a dione complex by a hydrogen rebound and a C−C bond cleavage. Kinetic isotope effects (k_H/k_D) for the electronic processes of the C−H bond dissociations calculated to be 4.9−7.4 at 300 K are in good agreement with experiment values of 2.8−9.0.

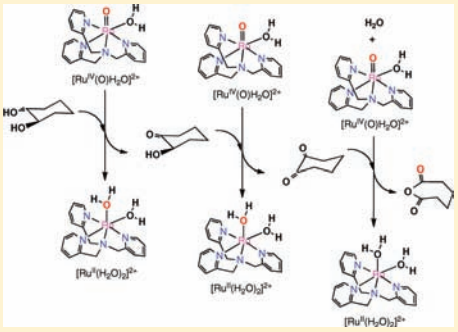

INTRODUCTION

The design of greener chemical processes has become a top priority in recent years. In this sense, studies on methods for highly selective and efficient conversion of abundant organic resources into valuable products with metal complexes as catalysts are very important.[1,2] High-valent metal−oxo species are often key intermediates in such catalytic reactions, for example, iron(IV)−oxo or the analogous ruthenium(IV)−oxo complexes. These complexes often mimic enzyme active centers responsible for biological oxidation and oxygenation of hydrocarbons.[3−5] Under experimental conditions these metal−oxo species can be generated using "peroxo shunt" with peroxides and H_2O_2. This is not always practical; therefore, exploring alternative strategies of formation is important. One possibility is to separate the oxidation step from the oxygen source. This strategy is inspired by biological examples, like the reaction center in Photosystem II. A tetranuclear manganese cluster in the oxygen-evolving complex (OEC) in Photosystem II is responsible for conversion of Mn−aqua to Mn−oxo species, which is responsible for dioxygen formation using water as an oxygen source.[6−9] This Mn−oxo complex has been proposed to be formed by proton-coupled electron transfer (PCET),[10] in which deprotonation of coordinated water and oxidation of the metal center are considered to occur in a concerted manner. A number of molecular catalysts have been reported for similar photochemical oxidation of water to dioxygen using water as an electron donor.[11−14] Ruthenium-based catalysts also have been reported to perform water oxidation, and mononuclear, dinuclear, and tetranuclear Ru complexes have been demonstrated to exhibit such reactivity.[15−23] Qualitative evidence for water oxidation by a dinuclear Ru complex has been presented by Meyer and coworkers.[15] One of the first examples of a ruthenium-based catalyst for water oxidation is the *cis,cis*-$[(bpy)_2(H_2O)Ru^{III}ORu^{III}(H_2O)(bpy)_2]^{4+}$ (bpy = 2,2′-bipyridine) complex with an oxo bridge

Received: March 8, 2011
Published: June 02, 2011

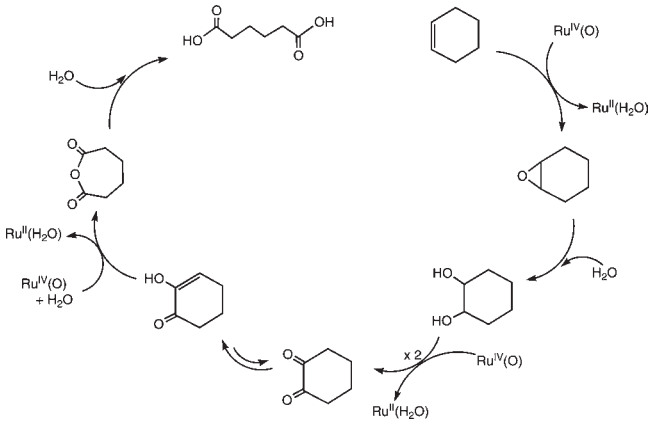

Figure 1. Proposed mechanism of cyclohexene to adipic acid catalyzed by Ru^{IV}−oxo complex.[27]

between the metals.[15a] More active dinuclear ruthenium water oxidation catalysts were developed by Tanaka's group[18] and Llobet's group.[19] Recently, the two groups independently reported a tetranuclear ruthenium cluster for water oxidation.[20,21] Thummel and co-workers[22] showed that mononuclear ruthenium complexes as well as dinuclear ruthenium complexes exhibit good catalytic activity with turnover numbers in the range of 20−260. In 2008 Meyer's group also suggested sustained catalytic water oxidation at a single ruthenium site.[23] Water oxidation mechanism involves formation of RuO species that can also catalyze oxidation of hydrocarbons.[24−26] Che et al.[24] reported catalytic oxidations of alkanes and alcohols mediated by ruthenium−oxo complexes with cerium(IV) ammonium nitrate as an oxidant in aqueous solution. They suggested that the reactions are fully consistent with a free radical process. On the other hand, Bryant, Matsuo, and Mayer[26] proposed that oxidation of cumene by $Ru^{IV}O$ species in acetonitrile solution occurs by hydrogen-atom transfer rather than nucleophile-assisted hydride transfer.

In this report we investigate a novel Ru^{IV}−oxo complex cation, $[Ru^{IV}(O)(tpa)(H_2O)]^{2+}$ (tpa = tris(2-pyridylmethyl)amine), first introduced by Kojima et al.[27] This complex can be formed using cerium(IV) as an oxidant and water as an oxygen source and perform a highly efficient and selective catalytic oxygenation of hydrocarbons in water. In this paper we focus on the 8-electron oxidation of cyclohexene to form adipic acid and reaction mechanism proposed by Kojima (Figure 1).[27] This catalytic cycle involves epoxidation of cyclohexene, hydrolysis of the epoxide to give cyclohexane-1,2-diol, the four-electron oxidation of the diol to give cyclohexane-1,2-dione, its subsequent Baeyer−Villiger-like oxidation to give an acid anhydride, and a final hydrolysis under strongly acidic conditions to give adipic acid. The analogous nonheme iron complex, $[Fe^{IV}(O)(tpa)(H_2O)]^{2+}$, has been previously characterized, and a similar reaction was reported with cerium(IV) ammonium nitrate as an oxidant.[28] Although they investigated the oxidation of cyclohexene by FeO species using UV−vis spectral changes, our knowledge on the mechanism of the direct oxidation of cyclohexene to adipic acid is rather limited despite the accumulation of many experimental facts.[29,30] The analogous catalytic oxidation of cyclohexene to adipic acid over an iron porphyrin complex has been reported by Zhong and co-workers.[31] A detailed theoretical analysis of this reaction was performed by Sieghban and co-workers,[32] who proposed a mechanism via two consecutive hydroxylation steps. In this model, one of the C−H abstractions is the rate-determining step.

There are several theoretical accounts discussing the oxidation of olefins, alcohols, and ketones by $Ru^{IV}O$ complexes. Cundari and Drago[33] investigated $Ru^{IV}O$-catalyzed epoxidation of ethylene using the semiemprical INDO/1 formalism. As demonstrated in their pioneering work, a great deal of attention has been focused on better understanding of the catalytic oxidation of organic compounds by $Ru^{IV}O$ species from a theoretical point of view.[34−36] Density functional theory (DFT) calculations[34,37] on high-valent ruthenium−oxo complexes have explained a number of experimental facts about ruthenium−oxo catalysts, i.e., (1) ruthenium−oxo catalysts are expected to lead to more stereoselective hydroxylations compared with the corresponding iron−oxo reactions,[38] (2) ruthenium−oxo catalysts should have larger turnover numbers compared with the iron−oxo analogue due to lesser production of suicidal side products that destroy the catalyst,[39] and (3) the ruthenium complex is more electrophilic than its iron analogue, having lower hydrogen abstraction barriers.[38] These three reasons make Ru-based catalysts a strong candidate for the selective and efficient functionalization of hydrocarbons. However, the reaction mechanism for oxidation of diol to acid anhydride catalyzed by a $Ru^{IV}O$ complex[27] is not fully understood. Since the oxidation mechanism of secondary alcohols to ketones by metal−oxo species leads to two possible reaction pathways with respect to the initial H-atom abstraction, we are particularly interested in the reaction mechanism for alcohol oxidation. Yoshizawa and Kagawa also investigated the selective oxidation of methanol mediated by the closely related bare FeO^+ ion in the gas phase from a theoretical viewpoint.[40] They suggested that the selective oxidation of alcohol by FeO^+ species involves multiple reaction pathways corresponding to cleavage of C−H, O−H, and C−O bonds. In this article, we present plausible mechanisms for conversion of cyclohexanediol to adipic anhydrate by a $[Ru^{IV}O(tpa)(H_2O)]^{2+}$ complex in solution. This theoretical study sheds new light on the C−H activation of diol, hydroxyketone, and diketone by the RuO species.

METHOD OF CALCULATION

Geometry optimization and transition-state search were performed using the hybrid (Hartree−Fock/DFT) B3LYP method.[41,42] In addition, the M06 method[43] was used as a complementary approach to the B3LYP results. The Hay−Wadt basis set[44] was used for Ru, the SDD basis set[45] for Ce, and the D95** basis set[46] for H, C, N, and O atoms. Vibrational frequencies were systematically computed in order to verify each optimized geometry corresponding to a local minimum with no imaginary frequency or a saddle point with only one imaginary frequency. Zero-point vibrational energy corrections were taken into account in calculating the total energies of the reaction species. Single-point calculations in aqueous solution were carried out on the basis of the gas-phase-optimized geometry for the adducts and corresponding transition states using the integral equation formalism of the polarizable continuum model (IEF-PCM).[47] The Gaussian 09 program package[48] was used for all DFT calculations.

RESULTS AND DISCUSSION

The $Ru^{IV}O$ complex is formed by oxidizing the Ru^{II}−bisaqua complex with Ce^{IV} in the following reaction

$$2Ce^{4+} + [Ru^{II}(tpa)(H_2O)_2]^{2+} \rightarrow 2Ce^{3+} + 2H^+ + [Ru^{IV}(O)(tpa)(H_2O)] \quad (1)$$

dx.doi.org/10.1021/ic200481n |*Inorg. Chem.* 2011, 50, 6200–6209

Scheme 1

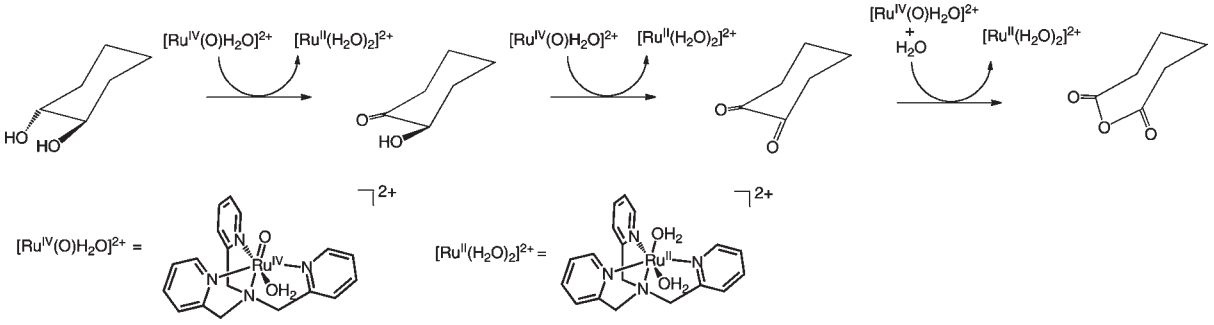

Cerium(IV) ammonium nitrate is used as a sacrificial reagent to maintain the catalytic cycle and regenerates $Ru^{IV}O$. Unfortunately, our efforts to correctly describe the thermochemistry of the oxidation step (1) with DFT calculations did not lead to success. One problem we faced is the accurate prediction of the solvation enthalpy of the two protons released. Thermodynamic estimations based on protonated solvent molecules (H_3O^+) can lead to unrealistic results. While there are sophisticated methods with promising results[49] to estimate the effect of solvation, application of them is out of the scope of the present paper.

We considered the conversion of cyclohexanediol to adipic anhydride by the $Ru^{IV}O$(tpa) complex, as indicated in Scheme 1. Dehydrogenation of cyclohexanediol with the $Ru^{IV}O$(tpa) complex is initiated by two H-atom abstractions, followed by formation of hydroxyketone and the Ru^{II}(tpa) complex. In the next step conversion of hydroxyketone to dione by another $Ru^{IV}O$(tpa) complex occurs. Finally, a third $Ru^{IV}O$(tpa) complex oxidizes the dione to form adipic anhydride.

$Ru^{IV}O$(tpa) Complex and Ru^{II}(tpa) Complex. The ground states of the $Ru^{IV}O$(tpa) and Ru^{II}(tpa) complexes are triplet and singlet,[27] respectively, as experimentally determined with the Evans method.[50] B3LYP and M06 calculations are consistent with the experiments and correctly predict the spin states for the both complexes. A calculated singlet−triplet gap, $\Delta E = E_S - E_T$, is 18.7 kcal/mol (B3LYP)/17.7 kcal/mol (M06) in the $Ru^{IV}O$(tpa) complex, whereas the same energy gap is −19.7 kcal/mol (B3LYP)/−17.7 kcal/mol (M06) in the Ru^{II}(tpa) complex. The energies calculated with the two DFT methods are essentially identical; therefore, to avoid unnecessary duplication of discussion we adopt the B3LYP results. The M06 energies are summarized in the Supporting Information.

The coordination environments in both Ru complexes are approximately octahedral. According to ligand field theoretical considerations, the four d electrons of the $Ru^{IV}O$(tpa) complex occupy the t_{2g} orbitals. With the Ru═O bond in the direction of the z axis, the d_{xy} orbital is doubly occupied, while the two unpaired electrons on the d_{yz} and d_{zx} orbitals form the triplet spin state. The six electrons of the Ru^{II} complex form a closed-shell singlet state with three pairs of electrons on the approximately 3-fold degenerate t_{2g} orbitals.

This orbital picture can be further refined if we compare it with the research of Carter and Goddard,[51] who predicted the general bonding character of the bare MO^+ ions from all-electron ab-initio-generalized valence bond calculations. They suggested that the bare RuO^+ ion forms a weak, reactive double bond with biradical character analogous to the bond in O_2. Since the oxo ligand has a strong interaction with the Ru center compared to the aqua ligand and the tpa ligand, we can expect that the Ru═O bond in the $Ru^{IV}O$(tpa) complex shows significant similarity to the bare RuO^+ ion. B3LYP calculations demonstrated that the two singly occupied orbitals (HOMO and HOMO−1) correspond to the π-antibonding orbitals formed by the 4d orbital of Ru and the 2p orbital of O, as shown in Figure 2. These results are consistent with calculated Mulliken spin densities of 0.98 in the Ru atom and 1.02 in the oxo ligand. Thus, the Ru and O atoms are spin carriers in the $Ru^{IV}O$(tpa) complex, and this radical character of the oxygen ligand may indicate high oxidation activity for the strong C−H bond of the substrate. Due to the strong biradical character, the Ru^{IV}═O(tpa) species can also be interpreted as an $Ru^{III}-O^{\bullet}$(tpa) species.[52] The computed bond dissociation energy (BDE) for the Ru−O bond is 86.2 kcal/mol, which is comparable to an experimental value of 88 ± 2 kcal/mol in the bare RuO^+ ions.[53]

Considering that the ground states of the Ru^{IV} and Ru^{II} complexes are triplet and singlet, respectively, there must be at least one crossing point between the triplet and the singlet potential energy surfaces during the oxidation process. Spin crossover that can occur near a crossing region of potential energy surfaces of different spin states has a significant effect on the reactivity of the $Ru^{IV}O$(tpa) complex with substrate.

Figure 3 shows optimized structures of the $Ru^{IV}O$ and the Ru^{II} complex. The $Ru^{IV}O$ complex includes an oxo ligand, an aqua ligand, and a tpa ligand. The Ru−O bond distances of the oxo ligand and the water ligand are 1.777 and 2.229 Å, respectively. The Ru−N distances in the tpa ligand range from 2.062 to 2.211 Å. The shortest Ru−N bond is located at the trans position of the water ligand, and the longest Ru−N bond is located at the trans position of the oxo ligand. The Ru^{II} complex has two aqua ligands and a tpa ligand. The Ru−O bond distances of the water ligands are 2.283 and 2.273 Å. The Ru−N distances for the tpa ligand range from 2.042 to 2.124 Å.

Oxidation of *trans*-Cyclohexanediol. Conversion of *trans*-cyclohexanediol to α-hydroxycyclohexanone is initiated by hydrogen abstraction either from a hydroxyl group or its adjacent carbon, leading to a radical intermediate. Thus, there are two possible reaction pathways in which the first steps are cleavage of a C−H bond (path 1) or an O−H bond (path 2). In path 1, a subsequent H-atom abstraction from a carbon atom of cyclohexanediol via a transition state results in formation of a radical intermediate. After the spin transition from the triplet state to the singlet state, according to the DFT calculations, this intermediate is transformed into a hydroxy ketone complex via no transition state. The last step is dissociation of the hydroxy ketone from the reduced Ru complex. In path 2, a H-atom abstraction from an

dx.doi.org/10.1021/ic200481n |*Inorg. Chem.* 2011, 50, 6200–6209

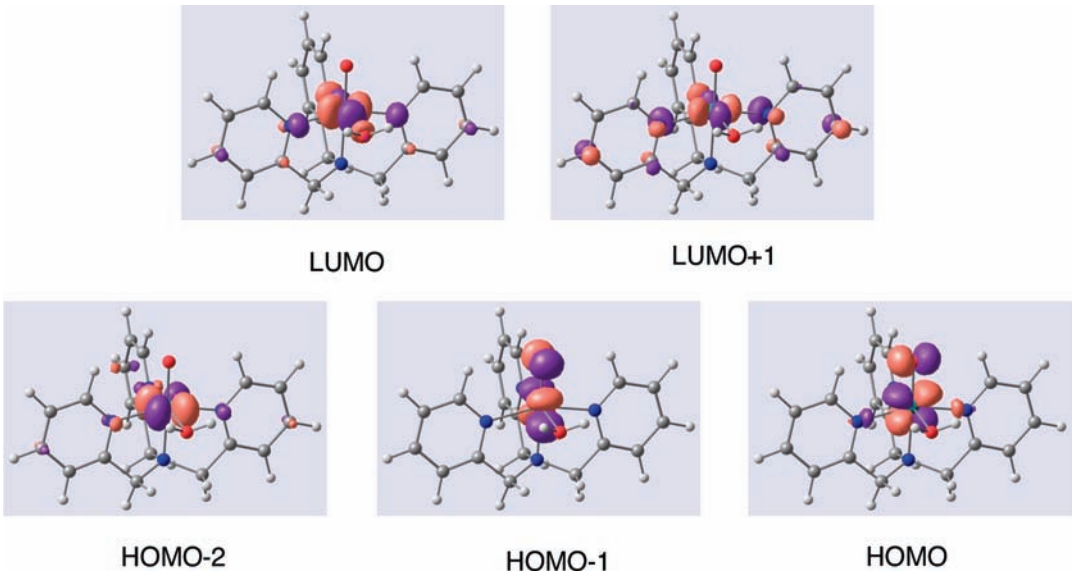

Figure 2. Computed molecular orbitals of the $Ru^{IV}O(tpa)$ complex in the triplet state. HOMO and HOMO−1 are singly occupied. The HOMO−2 orbital is doubly occupied.

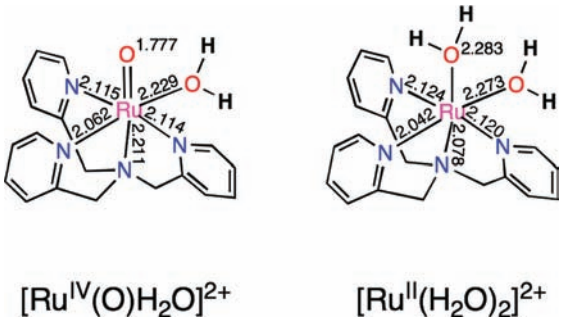

Figure 3. Optimized structures of the $Ru^{IV}O$ complex in the triplet state and the Ru^{II} complex in the singlet state.

oxygen atom of cyclohexanediol via a transition state results in formation of a radical intermediate. Calculations indicate that after a triplet−singlet spin transition this intermediate is transformed into a hydroxy ketone complex via a second transition state. DFT calculations suggested that path 2 involves two transition states, which is the significant difference between path 1 and path 2.

Figure 4 shows optimized structures and energies of the intermediates and transition states relative to the dissociation limit along path 1 and path 2 in the triplet state and the singlet state. The general profile of this diagram is downhill toward the product direction, and thus, the process is exothermic. It is therefore expected that this process should easily occur in solution. The $Ru^{IV}O$ complex and *trans*-cyclohexanediol form **1** with a binding energy of 13.3 kcal/mol in solution and 31.9 kcal/mol in the gas phase. The hydroxo groups of the substrate are anchored to the aqua ligand through two hydrogen bonds of 1.618 and 1.729 Å. In general, a cationic complex and neutral molecule have a strong binding energy. Thus, the binding energy of 31.9 kcal/mol comes from the Coulombic attraction rather than the hydrogen bonds. In path 1 the first transition state on the triplet surface, **TS1**, connects **1** and **Int1** with an imaginary frequency mode of 1729*i* cm^{-1}. This high frequency is a direct consequence of a C−H bond cleavage as well as an O−H bond formation, as the vibrational mode suggests. The transition structure involves a C−H bond of 1.354 Å and an O−H bond of 1.218 Å. These elongated bond distances of transition-state structure indicate cleavage of the C−H bond and formation of the O−H bond. The Ru−O bond distance is increased to 1.889 Å in **TS1** from 1.778 Å in **1**. One hydrogen bond increased to 1.947 Å in **TS1** from 1.729 Å in **1**. Another hydrogen bond of 1.655 Å remains almost unchanged. The C−H bond dissociation produces radical species; calculated spin densities of the carbon atom bonded to the hydroxo group are 0.42 in **TS1** and 0.85 in **Int1**. Thus, **Int1** is best described as a radical complex corresponding to the $Ru^{III}OH$ complex and a cyclohexanediol radical intermediate, which generates a triplet state from the coupling of the unpaired electron on the Ru with the electron of the cyclohexanediol radical. **Int1** is then transformed into **2** via no transition state after a spin transition from the triplet state to the singlet state, followed by dissociation of the complex into an α-keto-alcohol and the Ru^{II} complex. Since the structure of **2** shows two hydrogen bonds of 1.674 and 1.763 Å, the keto−alcohol moiety is strongly anchored by the two hydrogen bonds with the aqua ligands of the Ru^{II} moiety.

In path 2 the first transition state **TS2**−**1** is related to the H-atom abstraction from the OH group of *trans*-cyclohexanediol to form the intermediate complex **Int2**. **TS2**−**1** between **1** and **Int2** has an imaginary frequency mode of 829*i* cm^{-1} in the triplet state. The transition-state structure involves an O−H bond of 1.390 Å and a RuO−H bond of 1.075 Å. Considering the two bond distances along the reaction coordinate, **TS2**−**1** is a late transition state. The Ru−O bond distance is increased to 1.877 Å in **TS2**−**1** from 1.778 Å in **1**. One hydrogen bond increased to 1.778 Å in **TS2**−**1** from 1.618 Å in **1**, while the other hydrogen bond is shortened to 1.631 Å from 1.729 Å. **Int2** is also a radical complex corresponding to the $Ru^{III}OH$ complex and a radical intermediate. Calculated spin densities of the relevant oxygen are 0.46 in **TS2**−**1** and 0.80 in **Int2**. **Int2** undergoes a spin crossover from the triplet state to the open-shell singlet state to abstract the second hydrogen in **TS2**−**2**, which connects **Int2** and **2** as a transition state with an imaginary frequency mode of 714*i* cm^{-1}.

dx.doi.org/10.1021/ic200481n |*Inorg. Chem.* 2011, 50, 6200–6209

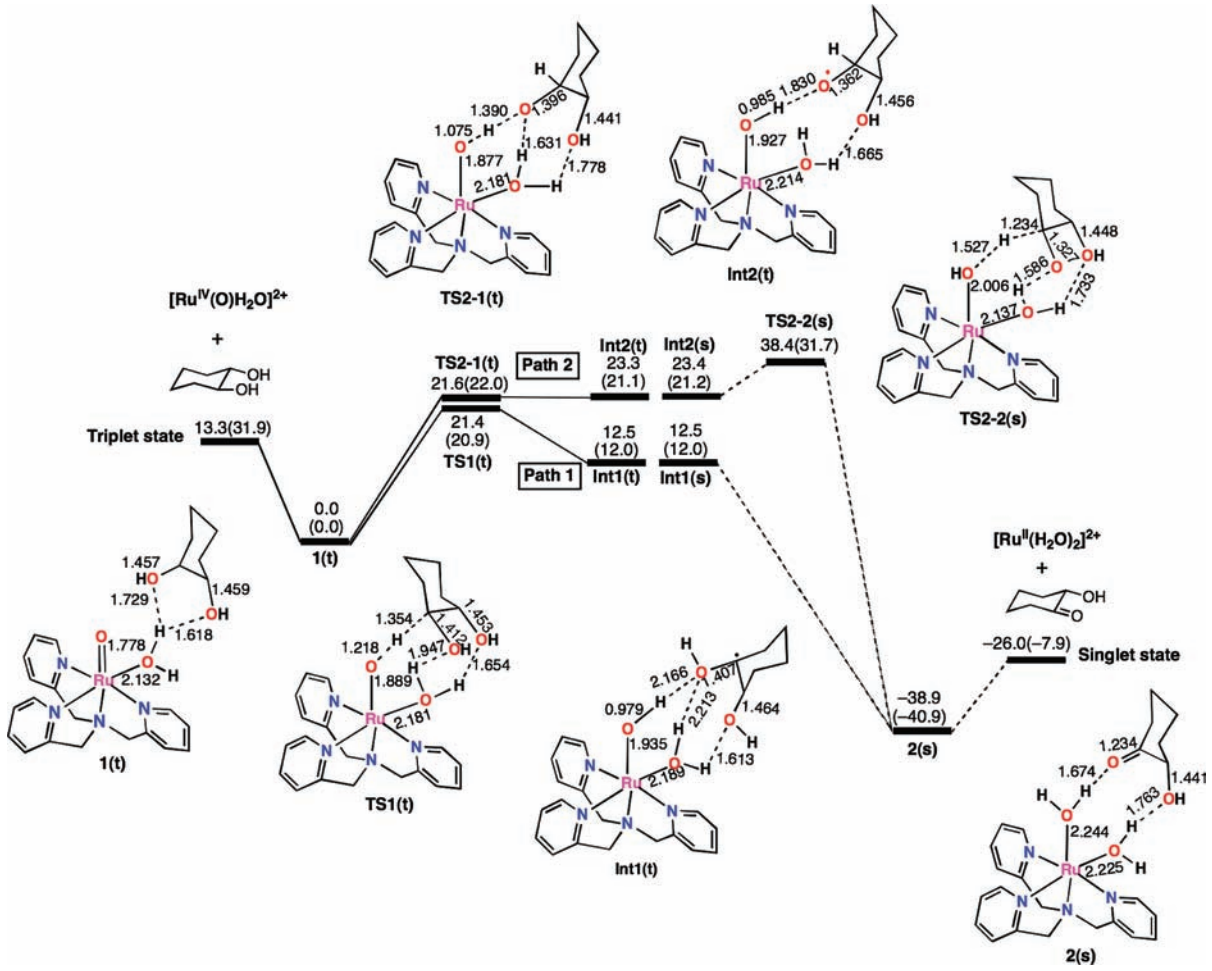

Figure 4. Computed energy diagrams and optimized structures for the oxidation of cyclohexanediol. Solid and dashed lines are, respectively, the energies of the triplet state and the singlet state. Values in the parentheses are the energies in vacuum. The energy of **Int1(s)** is calculated using the structure of **Int1(t)**. Units are in kcal/mol and Angstroms.

This transition state indicates a C−H bond of 1.234 Å and a RuO−H bond of 1.527 Å. The short C−H bond and the long O−H bond in **TS2−2** correspond to an early transition state, whereas **TS2−1** is a late transition state. Note that calculated $\langle S^2 \rangle$ values of 1.00 and 0.00 correspond to biradical species in the open-shell singlet state and nonradical species in the closed-shell singlet state, respectively. Therefore, a calculated $\langle S^2 \rangle$ value of 0.7932 in **TS2−2** suggests that an antiferromagnetic coupling between the two radical centers in the open-shell singlet state disappears with formation of **2** in the closed-shell singlet state.

Computed activation barriers of **TS1** and **TS2−1** are 21.4 and 21.6 kcal/mol relative to the reactant complex **1**, respectively. Although the two transition states are energetically comparable, the relative energies of the intermediates are quite different; **Int2** is energetically unstable compared to **Int1**. Moreover, there is a second transition state with an activation barrier of 15.0 kcal/mol in path 2, whereas there is no second transition state in path 1. After the first transition state the spin crossover from the triplet state to the open-shell singlet state plays an important role in formation of **2**. The potential energy diagrams demonstrate that the surface crossing between the triplet and the singlet states can occur in the vicinity of **Int1** and **Int2**. To consider the surface crossing we should find the minimum energy crossing seam point (MECP) on the two potential energy surfaces. A crossing seam with $3N - 7$ degrees of freedom was found, where different spin states reached the same energy. In fact, **Int1** and **Int2** are the optimized structures in the triplet spin state, and at the same time each point corresponds to a crossing seam between the triplet and singlet potential energy surfaces. Therefore, we regard **Int1** and **Int2** as an approximate MECP in each reaction pathway. The spin crossover is likely to occur in the vicinity of **Int1** and **Int2** corresponding to approximate MECPs. After spin crossover the singlet state **Int1** is not stable whereas **Int2** retains as a stable complex. Once the spin transition occurs, the singlet potential energy surface with **Int1** directly leads to formation of the relevant product. This kind of surface crossing and spin crossover in the activation of C−H bond are studied well in methane hydroxylation by FeO^+.[54] Harvey and co-workers[55] also pointed out that reaction rates of spin blocking strongly depend on details of the potential energy surfaces and of the topology associated with their crossing. These computational results lead us to conclude that path 1 is energetically favored in the oxidation of cyclohexanediol by the $Ru^{IV}O$(tpa) complex.

Oxidation of Hydroxy Cyclohexanone. Let us next look at the reaction of hydroxy cyclohexanone with the $Ru^{IV}O$(tpa) complex. The reaction proceeds through similar mechanisms as oxidation of *trans*-cyclohexanediol by the $Ru^{IV}O$(tpa) complex. There are also two possible H-atom abstractions with respect to

dx.doi.org/10.1021/ic200481n |*Inorg. Chem.* 2011, 50, 6200–6209

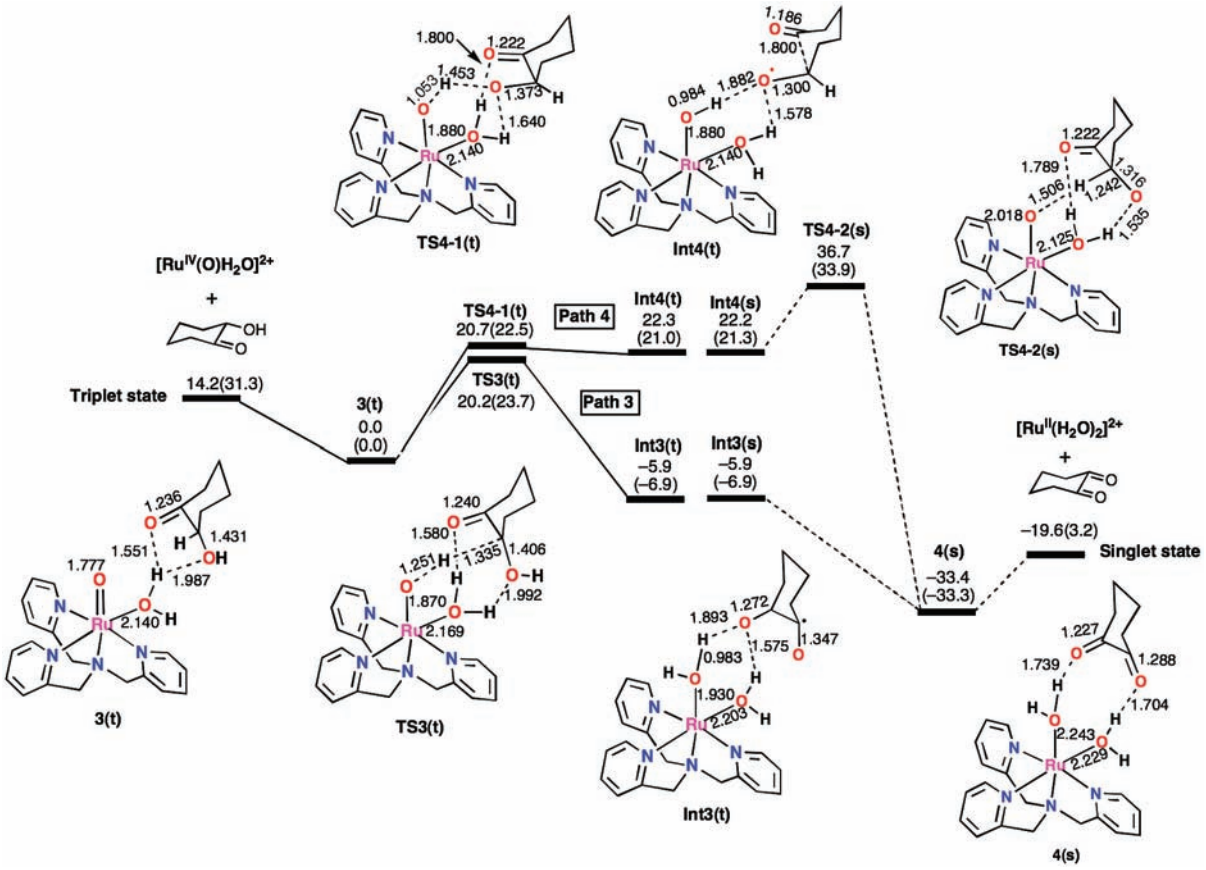

Figure 5. Computed energy diagrams and optimized structures for the oxidation of hydroxy cyclohexanone. Solid and dashed lines indicate the energy diagrams of the triplet state and singlet state, respectively. Values in parentheses are the energies in vacuum. The energy of **Int3(s)** is calculated using the structure of **Int3(t)**. Units are in kcal/mol and Angstroms.

C−H and O−H bonds, resulting in formation of cyclohexadione from the α-keto−alcohol. The two possible reaction pathways in which the $Ru^{IV}O$(tpa) complex can cleave a C−H bond or an O−H bond in the first step are shown in Figure 5. In path 3, the H-atom abstraction from a carbon atom of α-hydroxycyclohexanone via a transition state results in formation of a radical intermediate. After the spin transition from the triplet state to the singlet state, this intermediate is transformed into a dione complex via no transition state, followed by dissociation into cyclohexane-1,2-dione and the starting Ru^{II}−bisaqua complex. In path 4, the H-atom abstraction from the OH group of α-hydroxycyclohexanone via a transition state results in formation of a radical intermediate. After the spin transition from the triplet state to the singlet state, this intermediate is transformed into a dione complex via a second transition state. This dione complex dissociates into cyclohexane-1,2-dione and the Ru^{II}−bisaqua complex. A significant difference in this process is that path 4 involves two transition states, which is similar to the difference in the process between path 1 and path 2.

Optimized structures and energy diagrams of the intermediates and transition states along path 3 and path 4 are depicted in Figure 5, which also shows geometrical parameters and calculated energies relative to the reactant complex **3**. The general profile of this diagram is downhill toward the product direction. The $Ru^{IV}O$(tpa) complex and α-hydroxy-cyclohexanone form **3** with a binding energy of 14.2 kcal/mol in solution. The keto and hydroxy groups of the substrate are anchored to the aqua ligand of the Ru^{IV} moiety through hydrogen bonds of 1.551 and 1.987 Å, respectively. This former shorter hydrogen bond between the carbonyl group and the aqua ligand is quite short compared to the shortest hydrogen bond on **1** (1.618 Å).

In path 3 the first transition state **TS3** is responsible for the electronic process conducting the C−H bond dissociation of α-hydroxy cyclohexanone. **TS3** is a transition state, which connects **3** and **Int3** and shows an imaginary frequency mode of 1834*i* cm^{-1} in the triplet state. The vibrational mode suggests that a high frequency is a consequence of a C−H bond cleavage as well as O−H bond formation. The C−H bond and the O−H bond are calculated to be 1.335 and 1.251 Å, respectively, which is consistent with a transition-state structure leading to cleavage of a C−H bond and formation of an O−H bond. The Ru−O bond distance is increased from 1.777 Å in **3** to 1.930 Å in **Int3** via 1.870 Å in **TS3** showing that the Ru−O double bond is transformed to the Ru−O single bond. In **TS3** one hydrogen bond is elongated to 1.580 Å from 1.551 Å in **3**. The other hydrogen bond of 1.992 Å remains almost unchanged. **Int3** is a radical complex corresponding to the $Ru^{III}OH$ complex and a cyclohexane-1,2-dione radical intermediate in which the carbon atom bonded to the hydroxy group is the main spin carrier. Considering that the energy profile in the oxidation of α-hydroxy cyclohexanone is very similar to that in the oxidation of the diol described above, the spin transition in **Int3** is noteworthy. The potential energy surface in the vicinity of **Int3** is similar to that of **Int1.** Our computational results show that **Int3** in the singlet is

dx.doi.org/10.1021/ic200481n |*Inorg. Chem.* 2011, 50, 6200–6209

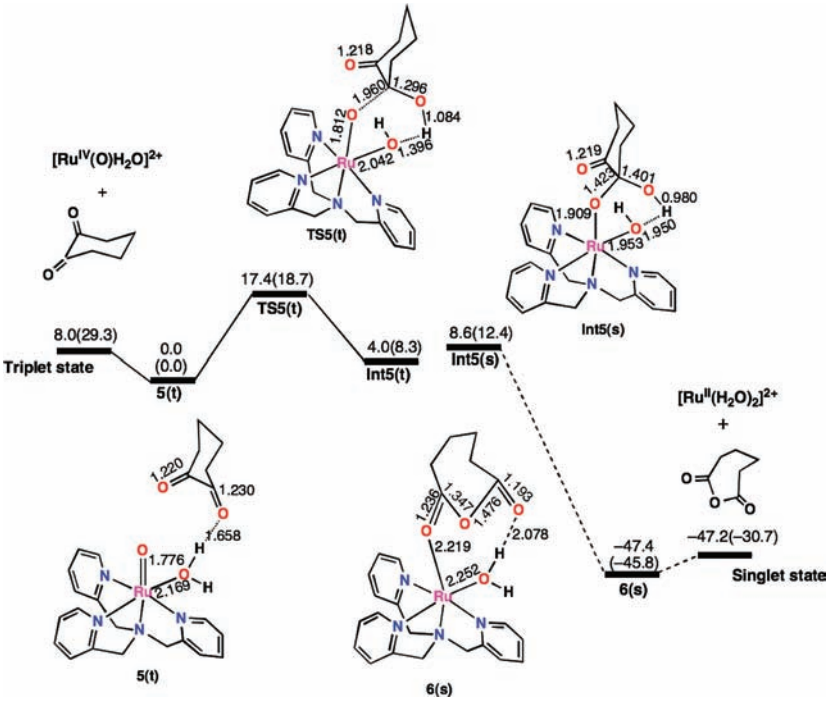

Figure 6. Computed energy diagram and optimized structures for the oxidation of cyclohexadione. Solid and dashed lines are, respectively, the energies of the triplet state and singlet state. Values in parentheses are the energies in vacuum. The energy of **Int5(s)** is calculated using the structure of **Int5(t)**. Units are in kcal/mol and Angstroms.

not stable. **Int3** is then transformed into **4** via no transition state after the spin crossover from the triplet state to the singlet state. The optimized structure of **4** is a complex consisting of the Ru^{II} moiety and cyclohexadione, which is strongly anchored by two hydrogen bonds of 1.739 and 1.704 Å, similar to those of **2**.

In path 4 the first transition state **TS4−1** is related to the H-atom abstraction from the OH group of α-hydroxy cyclohexanone to form the intermediate complex **Int4**. **TS4−1** connects **3** and **Int4** and exhibits an imaginary frequency mode of 455*i* cm^{-1} in the triplet state. The transition state has an O−H bond of 1.453 Å and a RuO−H bond of 1.053 Å. Although these bond distances are reasonable for a transition-state structure responsible for cleavage of a HCO−H bond and formation of a new O−H bond, the calculated RuO−H bond is nearly close to 0.984 Å corresponding to the RuO−H bond distance in **Int4**. Thus, **TS4−1** as well as **TS2−1** is regarded as a late transition state. In fact, **TS4−1** and **Int4** are close in energy. The Ru−O bond distance is increased to 1.880 Å in **TS4−1** from 1.777 Å in **3**. In **TS4−1** one hydrogen bond is elongated to 1.800 Å from 1.551 Å in **3** while the other hydrogen bond is reduced to 1.640 Å from 1.987 Å. **Int4** is a radical complex corresponding to the $Ru^{III}OH$ complex and a hydroxy cyclohexanone radical, in which the calculated spin densities in the triplet state are 0.20 in the oxygen atom of the carbonyl group and 0.38 in the oxygen atom of the hydrogen-abstracted point. The remaining spin density, 0.19, is on the carbon atom of the carbonyl group. We consider that the delocalized spin density should be related to the long C−C bond of 1.800 Å in the six-membered ring and the short C−O bond of 1.186 Å compared with the normal C−O double bond of 1.20 Å. **Int4** undergoes a spin crossover from the triplet state to the singlet state to follow the singlet energy surface into **TS4−2,** which involves the structure with the highest energy along path 4 and is responsible for the C−H bond dissociation. This second transition state connects **Int4** and **4** and shows an imaginary frequency mode of 720*i* cm^{-1}. The transition state indicates a C−H bond of 1.242 Å and a RuO−H bond of 1.506 Å. Thus, **TS4−2** also corresponds to an early transition state. Calculated spin densities in **TS4−2** of the open-shell singlet are distributed to be −0.83 in the RuO moiety, 0.51 at the oxygen atom of the radical center, and 0.14 at the hydrogen-abstracted carbon atom. After hydrogen migration, the electronic structure of the open-shell singlet state is transformed into that of the closed-shell singlet state with reduction of Ru^{III} to Ru^{II}.

The energy profile in the oxidation of α-hydroxy cyclohexanone is very similar to that in the oxidation of 1,2-cyclohexanediol. Computed activation barriers of **TS3** and **TS4−1** are 20.2 and 20.7 kcal/mol relative to the reactant complex **3**, respectively. There is no significant difference between the two activation barriers for the H-atom abstraction from **3**. Thus, the energies of the two intermediates are expected to determine the dominant pathway between path 3 and path 4. The relative energies of these intermediates are quite different; **Int3** and **Int4** are calculated to be −8.9 and 22.3 kcal/mol, respectively. **Int4** is energetically unstable compared to **Int3**. Moreover, there is a second transition state with an activation barrier of 14.5 kcal/mol in path 4, whereas there is no second transition state in path 3. Therefore, we conclude that path 3 is the dominant pathway in the oxidation of α-hydroxy cyclohexanone. In the final step release of cyclohexadione requires 34.6 kcal/mol in **4**.

Oxidation of 1,2-Diketone. We next consider insertion of an oxygen atom into 1,2-diketone by the $Ru^{IV}O$ complex via **TS5**, in which a nucleophilic attack of the oxo ligand occurs on the carbonyl carbon; simultaneously, the carbonyl oxygen accepts a proton to form a tetrahedral intermediate, **Int5**. Next is the spin crossover from the triplet state to the open-shell singlet, which induces the progress of the reaction; this chemical process

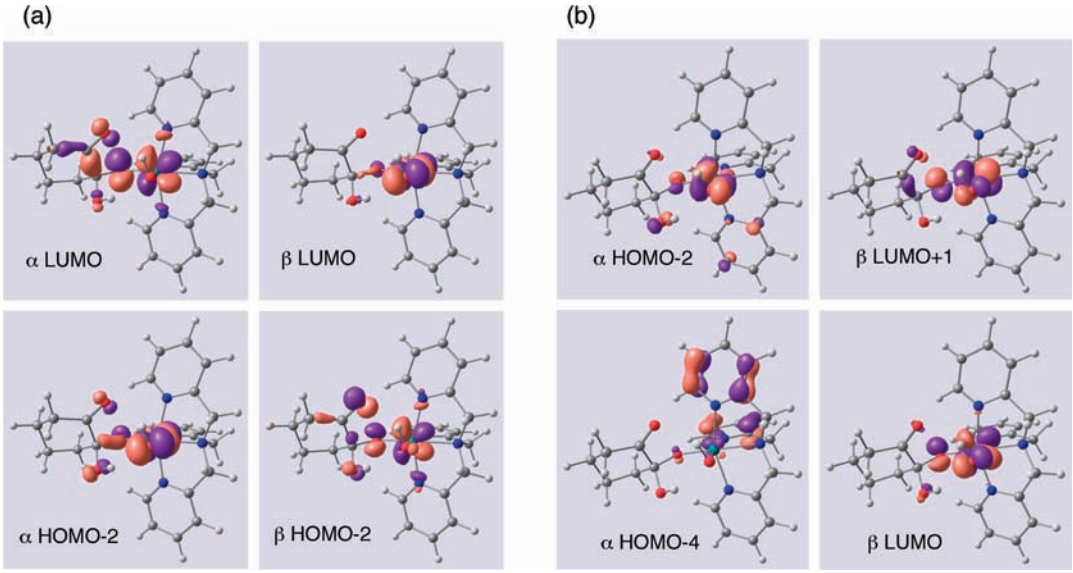

Figure 7. Magnetic molecular orbitals of the **Int5** complex in the (a) singlet state and (b) triplet state.

involves a hydrogen rebound and a concerted migration of oxygen with C−C bond cleavage of the adjacent carbon.

Figure 6 shows optimized structures and an energy diagram for insertion of an oxygen atom into diketone. The Baeyer−Villiger-like reaction is initiated by formation of the reactant complex **5** that involves diketone and $Ru^{IV}O$ complex with a binding energy of 8.0 kcal/mol. The reactant complex **5** involves one hydrogen bond between the aqua ligand and the carbonyl oxygen of 1.658 Å. This hydrogen bond plays an important role in the proton transfer from the aqua ligand. **TS5** is a transition state, in which the oxo ligand attack on the carbonyl carbon occurs simultaneously with the proton migration from the aqua ligand of the Ru moiety to the carbonyl oxygen atom. This reaction step requires an activation barrier of 17.4 kcal/mol with an imaginary frequency of 387*i* cm^{-1}. This transition state involves a $C_{carbonyl}$−O_{Ru} bond of 1.960 Å and O−H bonds of 1.396 and 1.084 Å, respectively. The relevant C−O bond distance in the carbonyl group increases from 1.230 Å in **5** to 1.401 Å in **Int5** via 1.296 Å in **TS5**. These bond distances are reasonable for a transition-state structure responsible for oxygen insertion and proton migration. Since the energy of **TS5** is 9.4 kcal/mol relative to the dissociation limit of $Ru^{IV}O$(tpa) and cyclohexadione, this process is expected to take place easily to form **Int5** under adiabatic conditions. Since **Int5** of the singlet state lies 4.6 kcal/mol above that of the triplet state, the surface crossing between the triplet and the singlet states occurs in the vicinity of **Int5**. Although **Int5** of the triplet state is a stable tetrahedral intermediate, the same geometry in the singlet state after the crossover is unstable; therefore, the single potential energy surface leads to formation of **6** concomitant with a hydrogen rebound and a C−C bond cleavage. Computational results show that the hydrogen shift is indispensable to the energy stabilization of **Int5**. Therefore, the aqua ligand plays an essential role in the oxygen insertion step through hydrogen migration. The final step is replacement of adipic anhydride by water to reproduce the Ru^{II}−bisaqua complex. The total reaction is computed to be exothermic by 55.2 kcal/mol. This reaction mechanism is similar to the catalytic oxidation of cyclohexane over heme as described by Siegbahn.[32] The calculated energy of the rate-determining step of the catalytic oxidation over iron is lower (about 20 kcal/mol) than the calculated value for the ruthenium catalyst. On the other hand, the selectivity of the iron-catalyzed reaction is low, which leads to almost 80% overoxidized byproducts.

The singlet spin state leads to cleavage of the Ru=O double bond and spin crossover. For this mechanism, therefore, the small energy gap between the singlet and the triplet states is an important factor in **Int5**. This energy gap is 4.6 kcal/mol, in contrast to the 18.7 kcal/mol stabilization of the triplet state in $Ru^{IV}O$(tpa) and 19.7 kcal/mol stabilization of the singlet state in Ru^{II}(tpa) (see above). The singlet state **Int5(s)** is an open-shell singlet with strong biradical character ($\langle S^2 \rangle$ = 0.98). The Mulliken spin density is +0.21 on the Ru and +0.27 and −0.32 on the oxygen atoms of the aqua and oxo ligands. The open-shell character of the singlet state comes from two half-occupied π^* orbitals: HOMO−2 and LUMO shown in Figure 7. The pair of α HOMO−2 and β LUMO and the pair of HOMO−2 and α LUMO are almost identical, and they correspond to a broken symmetry wave function of antiferromagnetically coupled pair of half spins. The triplet state in **Int5** corresponds to the ferromagnetic arrangements of the same spin pair, i.e., these orbitals become occupied in α space, and unoccupied in β space (see α HOMO−2, α HOMO−4 vs β LUMO, β LUMO+1). The small triplet−singlet energy gap therefore corresponds to the flipping between the antiferromagnetic and the ferromagnetic orientation of this pair of electrons.

Kinetic Isotope Effects (KIE). As the kinetic isotope effect is experimentally available for the reaction, we can compare them with KIE values corresponding to the proposed reaction mechanism. The rate-determining steps for path 1 and path 2 (path 3 and path 4) are the C−H bond dissociation steps with respect to **TS1** and **TS2**−**2** (**TS3** and **TS4**−**2**), respectively. Kinetic isotope effects (KIEs) are calculated using transition-state theory,[56,57] which lead to the following expression

$$\frac{k_H}{k_D} = \left(\frac{m_D^R m_H^\#}{m_H^R m_D^\#}\right)^{3/2} \left(\frac{I_{xD}^R I_{yD}^R I_{zD}^R}{I_{xH}^R I_{yH}^R I_{zH}^R}\right)^{1/2} \left(\frac{I_{xH}^\# I_{yH}^\# I_{zH}^\#}{I_{xD}^\# I_{yD}^\# I_{zD}^\#}\right)^{1/2} \frac{q_D^R q_H^\#}{q_H^R q_D^\#} \exp\left(-\frac{E_H^\# - E_D^\#}{RT}\right) \quad (2)$$

dx.doi.org/10.1021/ic200481n |*Inorg. Chem.* 2011, 50, 6200–6209

Table 1. Calculated k_H/k_D Values for the C−H Bond Dissociation in Transition States for the Oxidation of Substrates and an Experimental Value for the Oxidation of Methanol

T (K)	TS1[a]	TS2−2[b]	TS3[c]	TS4−2[d]	exp.
300	7.4	5.3	7.4	4.9	2.8[e] (9.0)[f]
350	5.6	4.2	5.5	3.9	
400	4.5	3.5	4.5	3.3	

[a] The D-labeled substrate is $C_6D_{10}(OH)_2$. [b] The D-labeled substrate is $C_6D_{10}(OH)O^{\bullet}$. [c] The D-labeled substrate is $C_6D_9(O)(OH)$. [d] The D-labeled substrate is $C_6D_9(O)O^{\bullet}$. [e] The complete result is included in the Supporting Information. [f] An experimental value in parentheses is from ref 58; the k_H/k_D value in the oxidation of methanol by $[Ru(O)(bpy)_2(py)]^{2+}$ (bpy is 2,2′-bipyridine and py is pyridine) is estimated using the D-labeled substrate of CD_3OH in the total reaction at 298 K.

where subscripts H and D denote quantities belonging to the hydrogen- and deuterium-substituted systems, respectively, superscripts R and # denote quantities belonging to the reactants and activation complex, q stands for the vibrational partition function, $I_{x(y,z)}$ are principal moments of inertia, m is molecular mass, and $E^{\#}$ is the activation barrier calculated with respect to the reactants in their respective ground states and includes zero-point vibrational energies (ZPE) and thermal corrections to finite temperature.

Table 1 summarizes computed values of k_H/k_D for the H-atom abstraction via transition states and an observed KIE at 298 K. The kinetic isotope effect in general significantly depends on temperature and the electronic process of the rate-determining step. Each transition state with respect to the H-atom abstraction is energetically the highest transition state in each pathway. Therefore, kinetic isotope effects in the electronic process give us important information on the bonding nature of the C−H bond adjacent to the hydroxyl groups. **TS1** and **TS3** are responsible for the H-atom abstraction of the C−H bond of each substrate. Computed k_H/k_D values of 7.38 in **TS1** and 7.38 in **TS3** show large kinetic isotope effects. The experimental KIE $(k[D]_{obs}/k[H]_{obs})$ of 2.8 is estimated by the concentration dependence of k_{obs} for the oxidation reaction and the change of absorbance at 620 nm upon oxidation reaction of CH_3OH and CD_3OD as substrates at variable concentrations in the presence of $[Ru^{IV}(O)(TPA)(H_2O)]^{2+}$ (0.33 mM) in H_2O at 298 K. Rocker and Meyer[58] observed KIE of 9 in the oxidation of methanol by $[Ru^{IV}(O)(bpy)_2(py)]^{2+}$ (bpy is 2,2′-bipyridine and py is pyridine) at 298 K. **TS2−2** and **TS4−2** are responsible for the H-atom abstraction of the O−H bond of each radical. Calculated KIE values of 5.28 in **TS2−2** and 4.87 in **TS4−2** at 300 K are relatively small compared to those of **TS1** and **TS3**. **TS2−2** and **TS4−2** afford imaginary frequencies of about $800i$ cm^{-1}, while **TS1** and **TS3** give rise to ones about $1800i$ cm^{-1}. The KIE values are consistent with the magnitude of the imaginary frequency because a high imaginary frequency tends to show an isolated C−H(D) bond dissociation mode in a transition state. Since our computed results indicated that **TS1** or **TS3** is the rate-determining step, the calculated KIEs are fully consistent with the observed KIE of 2.8−9.0 in the oxidation of methanol. These small KIEs indicate that the possibility of tunneling effects is not significant in the RuO system. In conclusion, experimental KIE values are consistent with the mechanism, where oxidation of the diol occurs along paths 1 and 3.

CONCLUSIONS

We studied the mechanism for conversion of 1,2-cyclohexanediol to adipic anhydride by a $Ru^{IV}O(tpa)$ complex. The whole reaction is divided into three processes: (1) α-hydroxy cyclohexanone is formed by dehydrogenation, (2) 1,2-cyclohexanedione is formed by dehydrogenation of α-hydroxy-cyclohexanone, and (3) adipic anhydride is formed by oxygenation of the dione. In each process the $Ru^{IV}O(tpa)$ complex performs a two-electron oxidation to form the $Ru^{II}(tpa)$ complex. The ground states of the $Ru^{IV}O(tpa)$ complex and the $Ru^{II}(tpa)$ complex are the spin triplet and singlet states, respectively. The homolytic bond cleavage leads to a biradical intermediate, in which the triplet and singlet potential energy surfaces are crossed. After spin inversion from the triplet state to the singlet state the second step occurs in the vicinity of the radical intermediate. These singlet−triplet spin crossovers play an essential role in the mechanism of oxidation. While the triplet−singlet energy gap is rather large both in the $Ru^{IV}O$ and in the Ru^{II} complexes, the intermediates where the spin crossover occurs have a very strong biradical character. The spin crossover is essentially a spin flip between an open-shell singlet and a triplet state, while the electrons remain on the same orbitals. Future studies will be focused on - characterization of surface crossing seams between the singlet and the triplet potential energy surfaces so that the possibility of spin inversion is maximized. In addition, the results presented herein clearly indicate that trapping intermediates by hydrogen bonding with the reactive species should be available to achieve multielectron oxidations even in aqueous media.

ASSOCIATED CONTENT

Supporting Information. Complete ref 48, and atomic Cartesian coordinates for all structures optimized in the present study. This material is available free of charge via the Internet at http://pubs.acs.org.

AUTHOR INFORMATION

Corresponding Author
*E-mail: kazunari@ms.ifoc.kyushu-u.ac.jp.

ACKNOWLEDGMENT

We are thankful for Grants-in-Aid for Scientific Research (Nos. 18GS0207, 21350035, 21750063, and 2245028) from the Japan Society for the Promotion of Science, the Kyushu University Global COE Project, the Nanotechnology Support Project, the MEXT Project of Integrated Research on Chemical Synthesis, CREST of the Japan Science and Technology Co-operation, and the Collaborative Research Program of Institute for Chemical Research, Kyoto University (No. 2010-23). T.K. also appreciates a support from The Asahi Grass Foundation.

REFERENCES

(1) Shilov, A. E.; Shul'pin, G. B. *Chem. Rev.* **1997**, *97*, 2879–2932.
(2) Punniyamurthy, T.; Velusamy, S.; Iqbal, J. *Chem. Rev.* **2005**, *105*, 2329–2363.
(3) *Cytochrome P450, Structure, Mechanism, and Biochemistry*; Ortiz de Montellano, P. R., Ed.; Springer: New York, 1995.
(4) Schlichting, I.; Berendzen, J.; Chu, K.; Stock, A. M.; Maves, S. A.; Benson, D. E.; Sweet, R. M.; Ringe, D.; Petsko, G. A.; Sligar, S. G. *Science* **2000**, *287*, 1615–1622.

(5) Poulos, T. L. *Philos. Trans. R. Soc. A* **2005**, *363*, 793–806.
(6) Wydrzynski, T. *Photosystem II: The Light-Driven Water: Plastoquinone Oxidoreductase*; Springer: New York, 2005.
(7) McEvoy, J. P.; Brudvig, G. W. *Chem. Rev.* **2006**, *106*, 4455–4483.
(8) Renger, G. *Photosynth. Res.* **2007**, *92*, 407–425.
(9) Hillier, W.; Messinger, J. In *The Catalytic Manganese Cluster, in Photosystem II: The Water/Plastoquinone Oxido-Reductase of Photosynthesis*; Wydrzynski, T., Satoh, K., Eds.; Kluwer Academic Publishers: Dordrecht, The Netherlands, 2005; pp 567−608.
(10) (a) Huynh, M. H. V.; Meyer, T. J. *Chem. Rev.* **2007**, *107*, 5004–5064. (b) Meyer, T. J.; Huynh, M. H. V.; Thorp, H. H. *Angew. Chem., Int. Ed.* **2007**, *46*, 5284–5304.
(11) Ramaraj, R.; Kira, A.; Kaneko, M. *Angew. Chem., Int. Ed. Engl.* **1986**, *25*, 825–827.
(12) (a) Ruettinger, W.; Dismukes, G. C. *Chem. Rev.* **1997**, *97*, 1–24. (b) Ruettinger, W. F.; Campana, C.; Dismukes, G. C. *J. Am. Chem. Soc.* **1997**, *119*, 6670–6671.
(13) Naruta, Y.; Sasayama, M.; Sasaki, T. *Angew. Chem., Int. Ed. Engl.* **1994**, *33*, 1839–1841.
(14) (a) Limburg, J.; Brudvig, G. W.; Crabtree, R. H. *J. Am. Chem. Soc.* **1997**, *119*, 2761–2762. (b) Limburg, J.; Vrettos, J. S.; Liable-Sands, L. M.; Rheingold, A. L.; Crabtree, R. H.; Brudvig, G. W. *Science* **1999**, *283*, 1524–1527. (c) Limburg, J.; Vrettos, J. S.; Chen, H.; dePaula, J. C.; Crabtree, R. H.; Brudvig, G. W. *J. Am. Chem. Soc.* **2001**, *123*, 423–430. (d) Tagore, R.; Crabtree, R. H.; Brudvig, G. W. *Inorg. Chem.* **2008**, *47*, 1815–1823.
(15) (a) Gersten, S. W.; Samuels, G. J.; Meyer, T. J. *J. Am. Chem. Soc.* **1982**, *104*, 4029–4030. (b) Gilbert, J. A.; Eggleston, D. S.; Murphy, W. R., Jr.; Geselowitz, D. A.; Gersten, S. W.; Hodgson, D. J.; Meyer, T. J. *J. Am. Chem. Soc.* **1985**, *107*, 3855–3864. (c) Chronister, C. W.; Binstead, R. A.; Ni, J.; Meyer, T. J. *Inorg. Chem.* **1997**, *36*, 3814–3815. (d) Lebeau, E. L.; Adeyemi, S. A.; Meyer, T. J. *Inorg. Chem.* **1998**, *37*, 6476–6484.
(16) Howells, A. R.; Sankarraj, A.; Shannon, C. *J. Am. Chem. Soc.* **2004**, *126*, 12258–12259.
(17) Hurst, J. K.; Zhou, J.; Lei, Y. *Inorg. Chem.* **1992**, *31*, 1010–1017.
(18) (a) Wada, T.; Tsuge, K.; Tanaka, K. *Angew. Chem., Int. Ed.* **2000**, *39*, 1479–1482. (b) Wada, T.; Tsuge, K.; Tanaka, K. *Inorg. Chem.* **2001**, *40*, 329–337. (c) Muckerman, J. T.; Polyansky, D.; Wada, T.; Tsuge, K.; Tanaka, K. *Inorg. Chem.* **2008**, *47*, 329–337.
(19) Sens, C.; Romero, I.; Rodriguez, M.; Llobet, A.; Parella, T.; Benet-Buchholz, J. *J. Am. Chem. Soc.* **2004**, *126*, 7798–7799.
(20) Geletii, Y. V.; Botar, B.; Kgerler, P.; Hillesheim, D. A.; Musaev, D. G.; Hill, C. L. *Angew. Chem., Int. Ed.* **2008**, *47*, 3896–3899.
(21) Sartorel, A.; Carraro, M.; Scorrano, G.; De Zorzi, R.; Geremia, S.; McDaniel, N. D.; Bernhard, S.; Bonchio, M. *J. Am. Chem. Soc.* **2008**, *130*, 5006–5007.
(22) (a) Zong, R.; Thummel, R. P. *J. Am. Chem. Soc.* **2005**, *127*, 12802–12803. (b) Deng., Z.; Tseng, H.-W.; Zong, R.; Wang, D.; Thummel, R. P. *J. Inorg. Chem.* **2008**, *47*, 1835–1848. (c) Tseng, H.-W.; Zong, R.; Muckerman, J. T.; Thummel, R. P. *J. Inorg. Chem.* **2008**, *47*, 11763–11773.
(23) (a) Concepcion, J. J.; Jurss, J. W.; Templeton, J. L.; Meyer, T. J. *Inorg. Chem.* **2008**, *130*, 16462–16463. (b) Chen, Z.; Concepcion, J. J.; Jurss, J. W.; Meyer, T. J. *Inorg. Chem.* **2009**, *47*, 15580–15581. (c) Concepcion, J. J.; Tsai, M.-T.; Muckerman, J. T.; Meyer, T. J. *J. Am. Chem. Soc.* **2010**, *132*, 1545–1557.
(24) Che, C.-M.; Cheng, K.-W.; Chan, M. C. W.; Lau, T.-C.; Mak, C.-K. *J. Org. Chem.* **2000**, *65*, 7996–8000.
(25) Bryant, J. R.; Matsuo, T.; Mayer, J. M. *Inorg. Chem.* **2004**, *43*, 1587–1592.
(26) Xia, Q.-H.; Ge, H.-Q.; Ye, C.-P.; Liu, Z.-M.; Su, K.-X. *Chem. Rev.* **2005**, *105*, 1603–1662.
(27) Hirai, Y.; Kojima, T.; Mizutani, Y.; Shiota, Y.; Yoshizawa, K.; Fukuzumi, S. *Angew. Chem., Int. Ed.* **2008**, *47*, 5772–5776.
(28) (a) Lim, M. H.; Rohde, J.-U.; Stubna, A.; Bukowski, M. R.; Costas, M.; Ho, R. Y. N.; Münck, E.; Nam, W.; Que, L., Jr. *Proc. Natl. Acad. Sci. U.S.A.* **2002**, *100*, 3665–3670. (b) Lee, Y.-M.; Dhuri, S. N.; Sawant, S. C.; Cho, J.; Kubo, M.; Ogura, T.; Fukuzumi, S.; Nam, W. *Angew. Chem., Int. Ed.* **2009**, *48*, 1803–1806.
(29) Chatterjee, D. *Catal. Surv. Asia* **2009**, *13*, 132–142.
(30) Meyer, T. J.; Huynh, M. H. V. *Inorg. Chem.* **2003**, *42*, 8140–8160.
(31) Yuan, Y.; Ji, H.; Chen, Y.; Han, Y.; Song, X.; She, Y.; Zhong, R. *Org. Process. Res. Dev.* **2004**, *8* (3), 418–420.
(32) Noack, H.; Georgiev, V.; Blomberg, M. R. A.; Siegbahn, P. E. M.; Johansson, A. J. *Inorg. Chem.* **2011**, *50*, 1194–1202.
(33) Cundari, T. R.; Drago, R. S. *Inorg. Chem.* **1990**, *29*, 3904–3907.
(34) (a) Sharma, P. K.; de Visser, S. P.; Ogliaro, F.; Shaik, S. *J. Am. Chem. Soc.* **2003**, *125*, 2291–2300. (b) Dhuri, S. N.; Seo, M. S.; Lee, Y.-M.; Hirao, H.; Wang, Y.; Nam, W.; Shaik, S. *Angew. Chem., Int. Ed.* **2008**, *47*, 3356–3359.
(35) Lujan, S.; Slocik, J. M.; Chattejee, D.; Mitra, A.; Shepherd, R. E. *Inorg. Chim. Acta* **2004**, *357*, 785–796.
(36) Zierkiewicz, W.; Privalov, T. *Dalton Trans.* **2006**, 1867–1874.
(37) Ogliaro, F.; de Visser, S. P.; Groves, J. T.; Shaik, S. *Angew. Chem., Int. Ed.* **2001**, *40*, 2874–2878.
(38) Groves, J. T.; Shalyaev, K.; Lee, J. In *The Porphyrin Handbook*; Kadish, K. M., Smith, K. M., Guilard, R., Eds.; Academic Press: New York, 2000; Vol. 4, pp 17−40.
(39) Ortiz de Montellano, P. R.; Beilan, H. S.; Kunze, K. L.; Mico, B. A. *J. Biol. Chem.* **1981**, *256*, 4395–4399.
(40) Yoshizawa, K; Kagawa, Y. *J. Phys. Chem. A* **2000**, *104*, 9347–9355.
(41) Becke, A. D. *Phys. Rev. A* **1988**, *38*, 3098–3100.
(42) Lee, C.; Yang, W.; Parr, R. G. *Phys. Rev. B* **1988**, *37*, 785–789.
(43) Zhao, Y.; Truhlar, D. G. *Theor. Chem. Acc.* **2008**, *120*, 215–241.
(44) Hay, P. J.; Wadt, W. R. *J. Chem. Phys.* **1985**, *82*, 299–310.
(45) Dolg, M.; Stoll, H.; Preuss, H. *Theor. Chim. Acta* **1993**, *85*, 441–450.
(46) Dunning, T. H.; Hay, P. J. In *Modern Theoretical Chemistry*; Schaefer, H. F., III, Ed.; Plenum: New York, 1976; Vol. 3, pp 1−27.
(47) (a) Miertu, S.; Scrocco, E.; Tomasi, J. *Chem. Phys.* **1981**, *55*, 117–29. (b) Cancès, E.; Mennucci, B.; Tomasi, J. *J. Chem. Phys.* **1997**, *107*, 3032–3041. (c) Mennucci, B.; Cancès, E.; Tomasi, J. *J. Phys. Chem. B* **1997**, *101*, 10506–10517.
(48) Frisch, M. J.; et al. *Gaussian 09*, revision A.02; Gaussian, Inc.: Wallingford, CT, 2004.
(49) Liu, S.; Schauer, C. K.; Pedersen, L. K. *J. Chem. Phys.* **2009**, *131*, 164107.
(50) Evans, D. F. J. *J. Chem. Soc.* **1959**, 2003.
(51) Carter, E. A.; Goddard, W. A., III *J. Phys. Chem.* **1988**, *92*, 2109–2115.
(52) Kojima, T.; Hayashi, K.; Iizuka, S.; Tani, F.; Naruta, Y.; Kawano, M.; Ohashi, Y.; Hirai, Y.; Ohkubo, K.; Matsuda, Y.; Fukuzumi, S. *Chem.—Eur. J.* **2007**, *13*, 8212–8222.
(53) Chen, Y.-M.; Armentrout, P. B. *J. Chem. Phys.* **1995**, *103*, 618–625.
(54) (a) Yoshizawa, K.; Shiota, Y.; Yamabe, T. *Chem.—Eur. J.* **1997**, *3*, 1160–1169. (b) Yoshizawa, K.; Shiota, Y.; Yamabe, T. *J. Am. Chem. Soc.* **1998**, *120*, 564–572. (c) Yoshizawa, K.; Shiota, Y.; Yamabe, T. *Organometallics* **1998**, *17*, 2825–2831. (d) Yoshizawa, K.; Shiota, Y.; Yamabe, T. *J. Chem. Phys.* **1999**, *111*, 538–545. (e) Shiota, Y.; Yoshizawa, K. *J. Am. Chem. Soc.* **2000**, *122*, 12317–12326. (f) Shiota, Y.; Yoshizawa, K. *J. Chem. Phys.* **2003**, *118*, 5872–5879. (g) Yoshizawa, K. *Acc. Chem. Res.* **2006**, *39*, 375–382.
(55) Carreón-Macedo, J.-L.; Harvey, J. N. *J. Am. Chem. Soc.* **2004**, *126*, 5789–5797.
(56) Eyring, H. *J. Chem. Phys.* **1935**, *3*, 107–115.
(57) Frost, A. A.; Pearson, R. G. *Kinetics and Mechanism*; Wiley: New York, 1961.
(58) Rocker, L.; Meyer, T. J. *J. Am. Chem. Soc.* **1987**, *109*, 746–754.